Supplementary Information for

Enhanced Voltammetric Anion Sensing at Halogen and Hydrogen Bonding Ferrocenyl SAMs

Robert Hein, Xiaoxiong Li, Paul D. Beer,* Jason J. Davis*

Department of Chemistry, University of Oxford, South Parks Road, Oxford OX1 3QZ, U. K.

E-mail: paul.beer@chem.ox.ac.uk, jason.davis@chem.ox.ac.uk

Table of Contents

S1 Procedures and Instrumentation

General Information

All commercially available chemicals and solvents were used as received without further purification. All hygroscopic TBA salts were stored in vacuum dessicators at room temperature. Dry solvents were degassed with N_2 and dried on a Mbraun MPSP-800 column. Ultrapure water was obtained from a Milli-Q system (18.2 MΩcm). Electrolyte and analyte solutions were prepared from analytical grade chemicals. Mass spectrometry was performed on a Bruker micrOTOF. NMR spectra were recorded on Bruker NMR spectrometers (AVIII HD 500 or AVIII HD 400). Chromatography was performed using silica gel (particle size: 40-63 µm) or preparative TLC plates (20 × 20 cm, 1 mm silica thickness).

Caution! Perchloric acid and perchlorate salts are toxic and can be powerful oxidisers and explosives and should be handled with care. Whenever applicable (i.e. if no (perchloric) acid is required for the voltammetric investigations), the use of hexafluorophosphate salts is recommended.

^{1}H NMR Titrations

In a typical titration experiment, the host solution (1.0 mM, 0.5 mL) was titrated with anion (as TBA salt) which was dissolved in the same deuterated solvent. Data fitting was carried out via OriginPro according to a 1:1 stoichiometric host-guest binding model.[1]

Electrochemical Studies and Titrations

All experiments were carried out using an Autolab potentiostat (Metrohm) in a three-electrode set-up. As working electrodes glassy carbon or gold disk electrodes were used. The counter electrode was a platinum wire. In all organic solvents a non-aqueous $Ag|AgNO_3$ reference electrode was used (10 mM $AgNO_3$ in 100 mM $TBAClO_4$ in ACN) and all potentials in organic solvents are reported with respect to this reference electrode. For the cleaning procedures in aqueous solvents a standard Ag|AgCl (3.4 M KCl) reference electrode was used.

CVs were recorded using a step potential of 2.4 mV and at a scan rate of 100 mV/s, unless otherwise noted. The electrochemical reversibility was assessed by recording CVs at varying scan rates (25, 50, 75, 100, 200, 400, 600 and 800 mV/s). SWVs were recorded using a step potential of 2 mV, a 20 mV amplitude and at a frequency of 25 Hz. All electrochemical titrations were followed by SWV. The receptors` half-wave potentials were determined as the peak potential by SWV.

For diffusive titrations a glassy carbon (GC) working electrode was utilised (3 mm diameter, BaSi). The receptor concentration was kept constant at 0.1 mM. In all cases the overall ion concentration was kept constant by titration of an initial host solution containing 100 mM $TBAClO_4$ with an anion solution in the same solvent system the same receptor concentration and 100 mM TBA-anion. Titrations of the surface-bound receptors were carried out analogously, in the additional presence of 0.1 mM $HClO_4$, as specified. The acid concentration was kept constant throughout. In most cases titrations were carried out up to an anion concentration of 50 mM. In a few cases the concentration range was limited to lower anion concentrations as a result of either: Overlapping redox activity of the anion and

the receptor (e.g. Br^- at SAMs), plateauing of the response at lower concentrations or poor reversibility/loss of redox activity at higher concentrations.

Electrode Cleaning

Glassy carbon electrodes: Mechanical polishing was carried out with alumina slurry (particle size: 0.05 µm; Buehler). Afterwards, the electrodes were briefly sonicated in EtOH/H_2O and then dried under N_2.

Gold electrodes (1.6 mm diameter, BaSi): Mechanical polishing was carried out as described above. Afterwards the electrodes were polished chemically by immersion in freshly prepared piranha acid (3:1 H_2SO_4/H_2O_2) for approx. 10 min. This was followed by electrochemical polishing in 0.5 M $KOH_{(aq)}$, between −0.7 and −1.7 V for approx. 1 h. Lastly the electrodes were electrochemically cleaned in 0.5 M $H_2SO_{4(aq)}$ between 0 and 1.5 V for at least 1 h. After rinsing with H_2O and EtOH the electrodes were dried under N_2 and used immediately. The electroactive surface area of the electrodes was determined from the CVs in 0.5 M $H_2SO_{4(aq)}$ according to standard procedures, utilising 559 µC/cm^2 as the conversion factor.[2]

SAM formation was carried out by immersing the freshly polished Au electrodes into a solution of **2.XB** or **2.HB** (0.25 mM in ACN) overnight in the dark. Subsequently the electrodes were rinsed with copious amounts of ACN, dried under N_2 and used immediately. SAMs for XPS or IR analyses were formed in the same manner on gold on silicon substrates (prepared in-house), which were cleaned by immersion in fresh piranha solution (see above) and copious rinsing with ACN, EtOH and H_2O.

X-ray Photoelectron Spectroscopy (XPS)

Samples were analysed using a Thermo Scientific K-Alpha XPS instrument equipped with a microfocussed monochromated Al X-ray source. The source was operated at 12 keV and a 400 micron spot size was used. The analyzer was operated at a constant analyser energy (CAE) of 200 eV for survey scans and 50 eV for detailed scans. Charge neutralization was applied using a combined low energy electron/ion flood source. Three spots per sample were measured.

Contact Angle Measurements

Static water contact-angle measurements were performed on a FTA1000B goniometer (First Ten Ångstroms) equipped with a manually operated microliter syringe. A sessile drop of deionised water (18.2 MΩ cm) was used as the wetting liquid. A point grey USB camera with a Navitar lens was used to capture videos at 61 frames per second. Data analysis was carried out with the FTA32 software and all droplets were fitted to a spherical model.

ATR-FTIR Spectroscopy

IR spectra were measured in transmission mode between 500 and 4000 cm^{-1} on an IRTracer-100 (Shimadzu). An average of 30 scans was recorded at a resolution of 0.5.

Data Analysis and Fitting

All data analysis and fitting was carried out with OriginPro 2017 unless otherwise noted. All binding constants are rounded to three significant figures.

It should be noted that all fits were carried out without any restriction of the parameters. In one case this affords a nonsensical, negative value for K_{Red} (Table 3). This is of course chemically impossible and purely arises from the fitting (*i.e.* this value afford the best mathematical fit to the Nernst model). If K_{Red} is restricted to 0 (the lowest chemically viable value) then an almost identical fit with slightly lower R^2 is obtained.

The conclusions that were drawn from the quantitative analyses presented in the main text, which subsequently aided in the development of the dielectric model, do not explicitly rely on the specific values (K_{Ox} and K_{Red}) that were obtained from fitting to eqn. 2. Specifically, the same conclusions can be drawn when analysing the trends of ΔE_{max} at 50 mM anion which is, according to the most general case (eqn. 1), directly proportional to the BEF as well (and thus also reports on the ratio of K_{Ox}/K_{Red}).

While eqn. 1 is valid in general (for both "continuous shift" as well as "two-wave" behavior), it only allows determination of the BEF at a plateauing response (ΔE_{max}), which, depending on the conditions and anion concentrations, may not be reached experimentally. Furthermore only the BEF is extractable, while the absolute values of K_{Ox} and K_{Red} cannot be determined. In contrast, eqn. 2 can be considered an extension of this model, which is valid when $[A^-] >> [H]$ and under continuous shift (fast exchange) conditions (which is the case throughout this work). For further discussions as well as a derivation of eqn. 2 the interested reader is referred to prior literature.[3, 4]

S2 Synthesis of Compounds

The synthetic route towards **1.XB/HB** and **2.XB/HB** is depicted in Scheme S1, commencing from 5-ferrocenylisophthalic acid (**3**), which was obtained in two steps as reported previously.[5] The conversion to its corresponding bis(acid chloride) followed by reaction with (iodo)propargylamine afforded the bis(iodo)alkynes **4a/b**. From **4a** receptors **1.HB** and **2.HB** were obtained in good yield by copper(I)-catalyzed azide-alkyne cycloaddition (CuAAC) with, respectively, octyl azide[6] or disulfide-azide[7] (Conditions A).

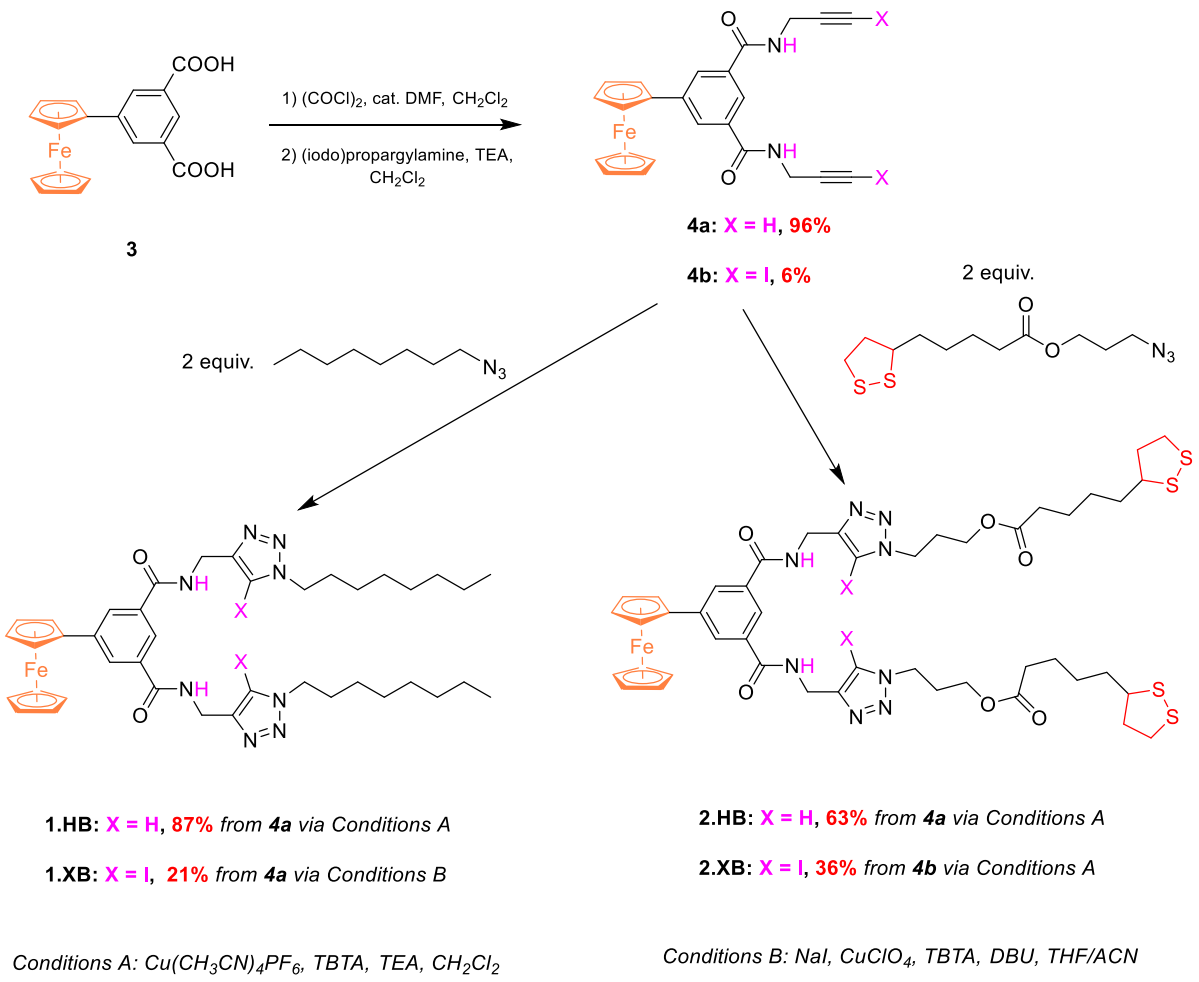

Scheme S1. Synthetic route towards halogen- and hydrogen-bonding redox active receptors **1.XB/HB** and **2.XB/HB**.

The synthesis of the XB analogues proved more challenging; **1.XB** was obtained from **4a** and octyl azide in a one pot reaction (conditions B),[8] albeit in only moderate yield, presumably due to partial deprotonation of the isophthalamide. We thus sought a different route towards the synthesis of disulfide-appended receptor **2.XB**, which was obtained from the isolated bis(iodoalkyne) **4b** under standard "click" conditions with disulfide-azide (conditions A).

Fc-isophthalamide-bis-alkyne 4a

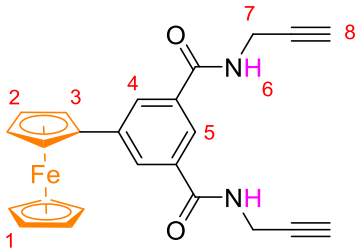

5-ferrocenyl isophthalic acid **3** (66 mg, 0.189 mmol) was suspended in 5 mL anhydrous DCM and cooled to 0 °C. A drop of DMF and $(COCl)_2$ (161 µL, 1.89 mmol) were then added. The mixture was stirred at rt for 4 h and then reduced *in vacuo*. The crude acid chloride was then redissolved in 3.5 mL anhydrous DCM and added dropwise to a solution of propargylamine (48 µL, 0.756 mmol) and TEA (66 µL, 0.473 mmol) in 5.5 mL anhydrous DCM under N_2. After 2 h the reaction was reduced *in vacuo* and **4a** isolated *via* silica gel column chromatography (2% MeOH/DCM) as an orange solid (77 mg, 0.181 mmol, 96%).

^{1}H NMR: (500 MHz, $CDCl_3$): δ 8.00 (2H, s, H^4), 7.96 (1H, s, H^5), 6.98 (2H, t, J = 5.0 Hz, H^6), 4.67 (2H, t, J = 1.6 Hz, H^3), 4.35 (2H, t, J = 1.6 Hz, H^2), 4.26 (4H, m, 4.26, H^7), 4.00 (5H, s, H^1), 2.30 (2H, t, J = 2.5 Hz, H^8). **^{13}C NMR:** (126 MHz, $CDCl_3$): δ 166.7, 141.6, 134.2, 127.7, 122.3, 82.7,

79.3, 72.1, 69.8, 66.7, 29.9. **ESI-MS:** m/z calcd. for $C_{24}H_{20}O_2N_2FeNa$ [M+Na$^+$] 447.07664, found: 447.07629.

Fc-isophthalamide-bis-iodoalkyne 4b

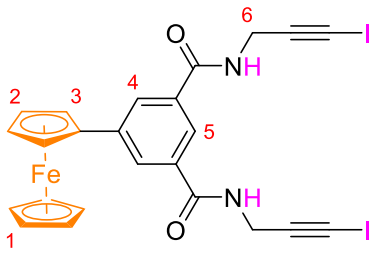

5-ferrocenyl isophthalic acid **3** (55 mg, 0.157 mmol) were converted to the corresponding acid chloride as described directly above (synthesis of **4a**). The crude acid chloride was dissolved in 5 mL anhydrous DCM and added dropwise to a solution of iodopropargylamine (86 mg, 0.471 mmol; freshly prepared according to literature procedure)[9] and TEA (0.3 mL, 2.15 mmol) in 10 mL anhydrous DCM under N_2. After 16 h the reaction mixtures was washed with H_2O twice and dried over $MgSO_4$. **4b** was then isolated *via* preparative TLC (1.5% MeOH/DCM) as an orange solid (6 mg, 8.9 µmol, 6%).

^{1}H NMR: (400 MHz, $CDCl_3$/MeOD 1:1): δ 8.09 (2H, d, *J* = 1.7 Hz, H^4), 8.02 (1H, t, *J* = 1.6 Hz, H^5), 4.79 (2H, t, *J* = 1.9 Hz, H^3), 4.37 (2H, t, *J* = 1.9 Hz, H^2), 4.33 (4H, s, H^6), 4.03 (5H, s, H^1). **^{13}C NMR:** (126 MHz, $CDCl_3$/MeOD 1:1): δ 168.1, 142.0, 134.7, 128.4, 123.5, 89.6, 83.6, 70.2, 70.2, 67.2, 31.7. **ESI-MS:** m/z calcd. for $C_{24}H_{18}O_2N_2FeI_2$ [M$^+$] 675.88106, found: 675.87975.

Fc-isophthalamide-bis-octyl-triazole 1.HB

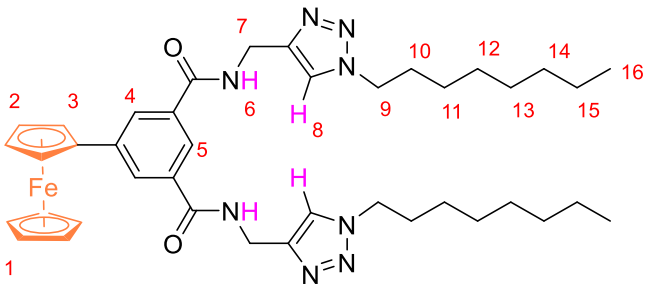

Fc-isophthalamide-bis-alkyne **4a** (73 mg, 0.172 mmol), octyl azide (59 mg, 0.3785 mmol), $Cu(CH_3CN)_4PF_6$ (13 mg, 0.0344 mmol), TBTA (9 mg, 0.0172 mmol) and TEA (35 mg, 0.344 mmol) were dissolved in 2 mL anhydrous DCM and reacted under N_2 for 47 h. The organic phase then washed with aq. NH_4OH twice, once with brine and dried over $MgSO_4$. **1.HB** was then isolated by silica gel column chromatography (5% MeOH/DCM) as an orange solid (110 mg, 0.150 mmol, 87%).

^{1}H NMR: ($CDCl_3$, 500 MHz): δ 8.27 (2H, t, *J* = 5.3 Hz, H^6), 8.12 (2H, s, H^4), 8.09 (1H, s, H^5), 7.70 (2H, s, H^8), 4.68 (6H, m, H^3+ H^7), 4.34 (6H, H^2 + H^9), 3.98 (5H, s, H^1), 1.88 (4H, quint., *J* = 6.9 Hz, H^{10}), 1.34 – 1.26 (20H, m, $H^{11\text{-}15}$), 0.86 (6H, t, *J* = 7.2 Hz, H^{16}). **^{13}C NMR:** ($CDCl_3$, 126 MHz): δ 165.9, 143.9, 140.2, 133.3, 127.0, 122.0, 121.1, 82.0, 68.7, 68.6, 65.7, 49.5, 34.4, 30.7, 29.2, 28.0, 27.9, 25.5, 21.6, 13.0. **ESI-MS:** m/z calcd. for $C_{40}H_{55}O_2N_8Fe$ $[M+H^+]$ 735.37919, found: 735.37879.

Fc-isophthalamide-bis-octyl-iodotriazole 1.XB

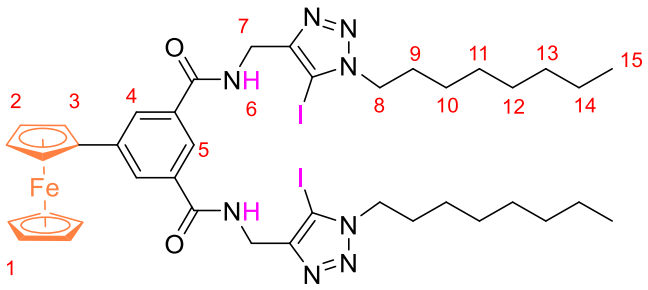

To a solution of octyl azide (74 mg, 0.48 mmol) in 2 mL THF was added $Cu(ClO_4)_2 \cdot 6H_2O$ (356 mg, 0.96 mmol) and NaI (288 mg, 1.92 mmol). The mixture was left to stir in the dark for 5 min before TBTA (13 mg, 0.025 mmol) was added. DBU (73 mg, 0.48 mmol) dissolved in 1 mL CH_3CN was added followed by addition of a solution of **4a** (101 mg, 0.24 mmol) in 1 mL CH_3CN. The reaction mixture was stirred at rt for 48 h. Subsequently, the mixture was washed with an EDTA solution (20 mL x 3), H_2O (3 x 30 mL) and then dried over $MgSO_4$. The solvent was removed *in vacuo* to afford a yellow solid. Purification of the compound was achieved by preparative TLC (3% MeOH/DCM) to afford **1.XB** as a yellow solid (50 mg, 0.05 mmol, 21%).

^{1}H NMR: ($CDCl_3$, 500 MHz): δ 8.04 (2H, s, H^4), 8.01 (1H, s, H^5), 7.46 (2H, t, J = 5.5 Hz, H^6), 4.68 (6H, m, $H^3 + H^7$), 4.34 (6H, $H^2 + H^8$), 4.00 (5H, s, H^1), 1.89 (4H, quint., J = 7.3 Hz, H^9), 1.34 – 1.26 (20H, m, $H^{10\text{-}14}$), 0.88 (6H, t, J = 7.2 Hz, H^{15}). **^{13}C NMR:** ($CDCl_3$, 126 MHz): δ 166.7, 148.0, 141.3, 134.4, 127.8, 122.3, 83.0, 78.7, 69.7, 66.8, 51.0, 36.1, 31.7, 29.9, 29.0, 29.0, 26.4, 22.6, 14.1. **ESI-MS:** m/z calcd. for $C_{40}H_{52}O_2N_8FeI_2Na$ [M+Na$^+$] 1009.15442, found: 1009.15386.

Fc-isophthalamide-bis-disulfide-triazole 2.HB

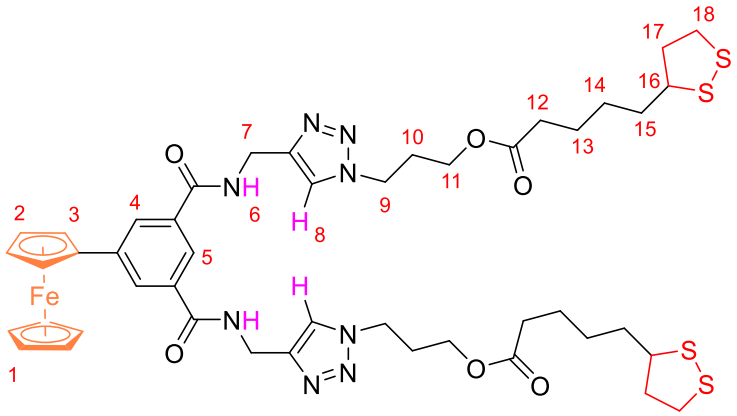

Fc-isophthalamide-bis-alkyne **4a** (50 mg, 0.118 mmol), disulfide-azide (75 mg, 0.259 mmol), $Cu(CH_3CN)_4PF_6$ (9 mg, 0.0236 mmol), TBTA (6 mg, 0.0118 mmol) and TEA (24 mg, 0.236 mmol) were dissolved in 3 mL anhydrous THF and reacted under N_2 in the dark for 16 h. DCM was then added and the organic phase was washed with aq. NH_4OH twice, once with brine and dried over $MgSO_4$. **2.HB** was then isolated by silica gel column chromatography (6% MeOH/DCM) as an orange solid (75 mg, 0.0748 mmol, 63%).

^{1}H NMR: ($CDCl_3$, 500 MHz): δ 8.13 – 8.04 (4H, m, H^4 + H^6), 8.02 (1H, t, J = 1.7 Hz, H^5), 7.73 (2H, s, H^8), 4.72 – 4.62 (6H, m, H^3+ H^7), 4.45 (4H, t, J = 7.0 Hz, H^9), 4.32 (2H, t, J = 1.8 Hz, H^2), 4.08 (4H, t, J = 6.0 Hz, H^{11}), 3.98 (5H, s, H^1), 3.54 (2H, dq, J = 8.5, 6.3 Hz, H^{16}), 3.24 – 2.99 (4H, m, H^{18}), 2.43 (2H, tt, J = 12.5, 6.0 Hz, H^{17}), 2.31 (4H, t, J = 7.4 Hz, H^{12}), 2.24 (4H, q, J = 6.6 Hz, H^{10}), 1.88 (2H, dq, J = 13.6, 6.9 Hz, H^{17}), 1.77 – 1.55 (8H, m, H^{13} + H^{15}), 1.52 – 1.34 (4H, m, H^{14}). **^{13}C NMR:** ($CDCl_3$, 126 MHz): δ 173.3, 167.0, 145.0, 141.3, 134.3, 127.9, 123.4, 122.2, 83.0, 69.7, 69.6, 66.7, 60.8, 56.3, 47.3, 40.3, 38.5, 35.4, 34.6, 33.9, 29.37, 28.7, 24.6. **ESI-MS:** m/z calcd. for $C_{46}H_{58}O_6N_8FeS_4$ [M^+] 1002.27061, found: 1002.27081.

Fc-isophthalamide-bis-disulfide-iodotriazole 2.XB

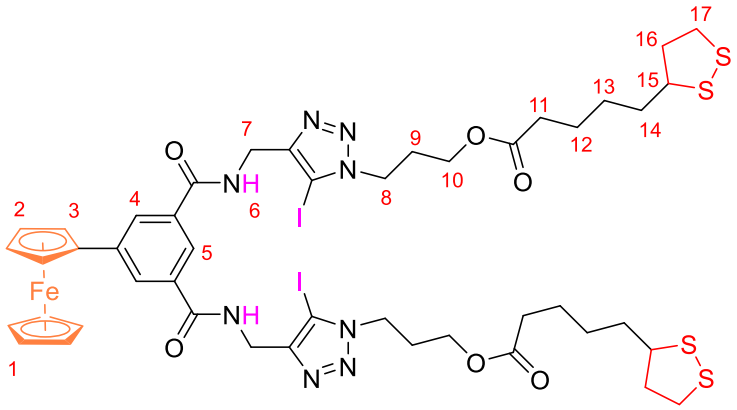

Fc-isophthalamide-bis-iodoalkyne **4b** (6 mg, 8.9 µmol), disulfide-azide (8 mg, 27.6 µmol), $Cu(CH_3CN)_4PF_6$ (13 mg, 0.0344 mmol), TBTA (cat.) and TEA (1 drop) were dissolved in 2 mL anhydrous DCM and reacted under N_2 in the dark for 24 h. The organic phase then washed with aq. NH_4OH twice, once with water and dried over $MgSO_4$. **2.XB** was then isolated by preparative TLC (5% MeOH/DCM) as an orange solid (4 mg, 3.2 µmol, 36%).

^{1}H NMR: ($CDCl_3$, 500 MHz): δ 8.07 (2H, d, *J* = 1.6 Hz, H^4), 7.98 (1H, t, *J* = 1.6 Hz, H^5), 7.05 (2H, t, *J* = 5.2 Hz, H^6), 4.82 – 4.65 (6H, m, H^3+ H^7), 4.49 (4H, t, *J* = 7.1 Hz, H^8), 4.44 – 4.34 (2H, m, H^2), 4.14 (4H, t, *J* = 6.0 Hz, H^{10}), 4.04 (5H, s, H^1), 3.56 (2H, dd, *J* = 8.4, 6.1 Hz, H^{15}), 3.22 – 3.05 (4H, m, H^{17}), 2.46 (2H, m, H^{16}), 2.37 – 2.25 (8H, m, H^9+ H^{11}), 1.98 – 1.85 (2H, m, H^{16}), 1.75 – 1.62 (8H, m, H^{12} + H^{13}), 1.55 – 1.39 (4H, m, H^{13}). **^{13}C NMR:** ($CDCl_3$, 126 MHz): δ 173.2, 166.5, 148.2, 141.6, 134.4, 127.8, 122.1, 82.9, 79.2, 69.8, 69.7, 66.81, 60.7, 56.4, 47.8, 42.3, 38.5, 36.1, 34.6, 34.0, 29.0, 28.8, 24.6. **ESI-MS:** m/z calcd. for $C_{46}H_{56}O_6N_8S_4FeI_2Na$ [$M+Na^+$] 1275.05834, found: 1275.05200.

S3 ^{1}H NMR Anion Binding Studies

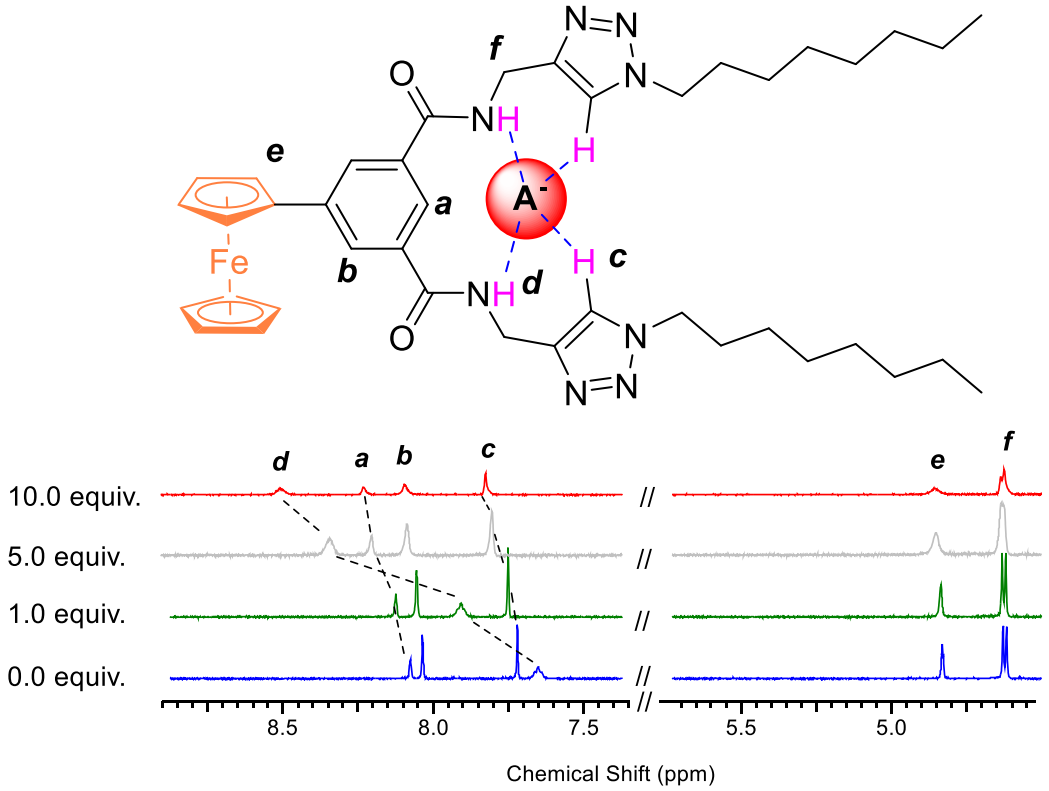

Figure S1. Partial ^{1}H NMR spectra of receptor **1.HB** in CD_3CN in the presence of 0.0, 1.0, 5.0 and 10.0 equivalents of $TBAHSO_4$. As only protons a, c and d display significant perturbations, anion binding in the central cavity *via* multiple convergent HB´s (blue dashed lines) can be inferred as schematically depicted.

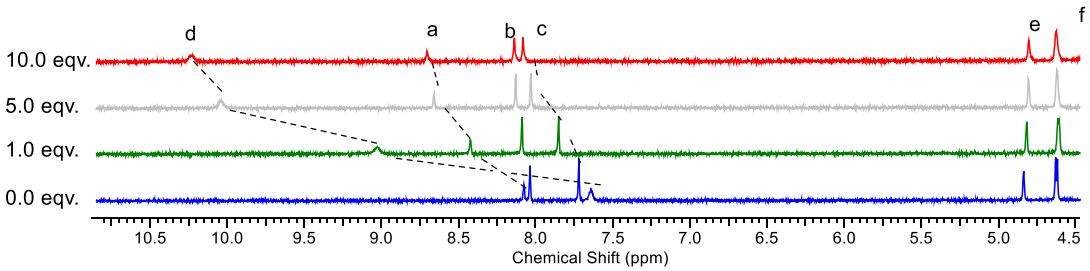

Figure S2. Partial ^{1}H NMR spectra of receptor **1.HB** in CD_3CN in the presence of 0.0, 1.0, 5.0 and 10.0 equivalents of $TBAH_2PO_4$ (400 MHz, 298 K).

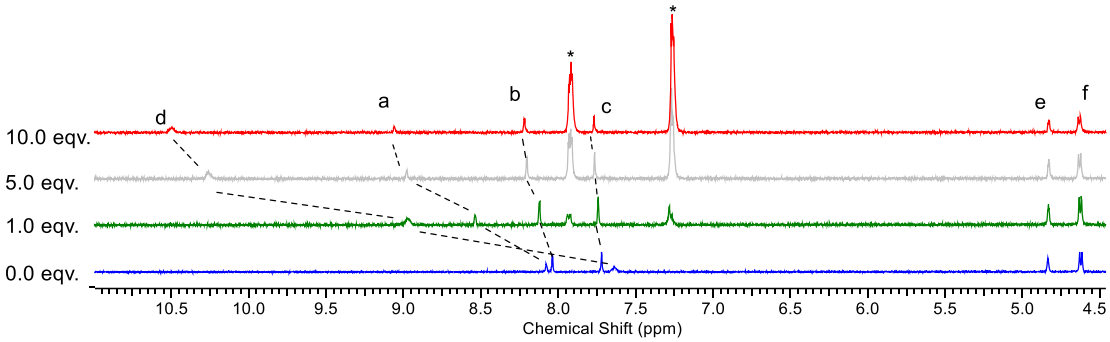

Figure S3. Partial ^{1}H NMR spectra of receptor **1.HB** in CD_3CN in the presence of 0.0, 1.0, 5.0 and 10.0 equivalents of of TBAbenzoate (400 MHz, 298 K, *aromatic signals of benzoate).

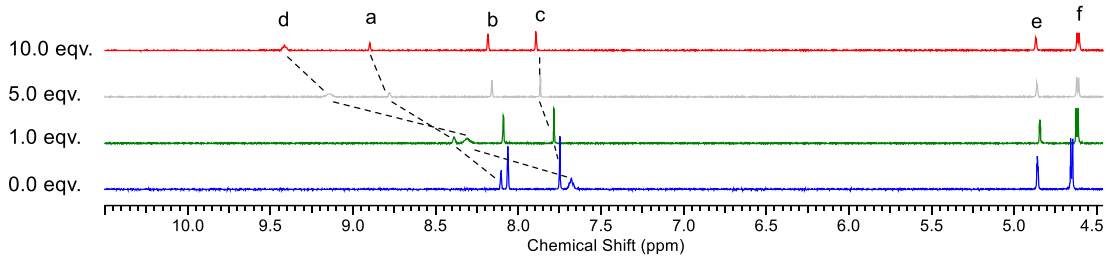

Figure S4. Partial ^{1}H NMR spectra of receptor **1.HB** in CD_3CN in the presence of 0.0, 1.0, 5.0 and 10.0 equivalents of TBACl (400 MHz, 298 K).

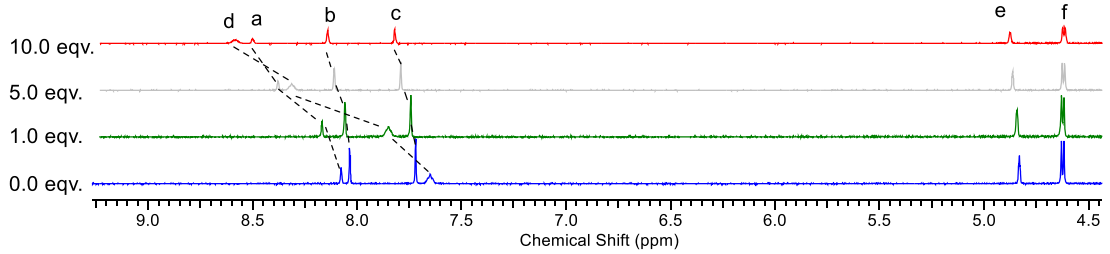

Figure S5. Partial ^{1}H NMR spectra of receptor **1.HB** in CD_3CN in the presence of 0.0, 1.0, 5.0 and 10.0 equivalents of TBABr 400 MHz, 298 K).

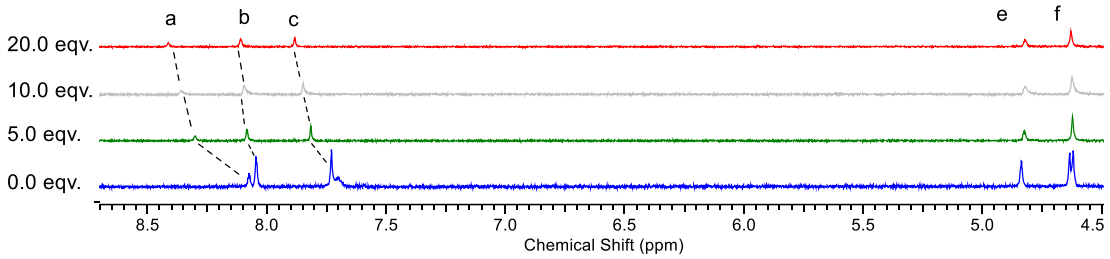

Figure S6. Partial ^{1}H NMR spectra of receptor **1.HB** in CD_3CN/D_2O (99:1 *v*/*v*) in the presence of 0.0, 1.0, 5.0 and 10.0 equivalents of $TBAH_2PO_4$ (400 MHz, 298 K).

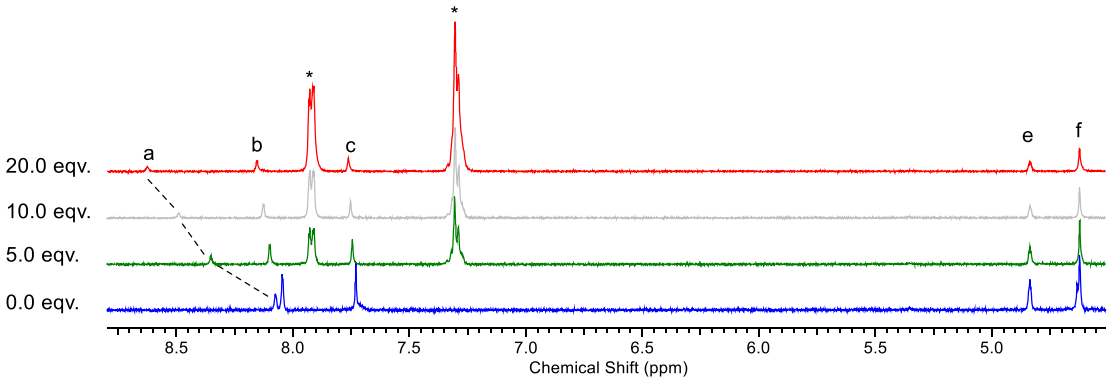

Figure S7. Partial ^{1}H NMR spectra of receptor **1.HB** in CD_3CN/D_2O (99:1 *v*/*v*) in the presence of 0.0, 1.0, 5.0 and 10.0 equivalents of TBAbenzoate (400 MHz, 298 K, *aromatic signals of benzoate).

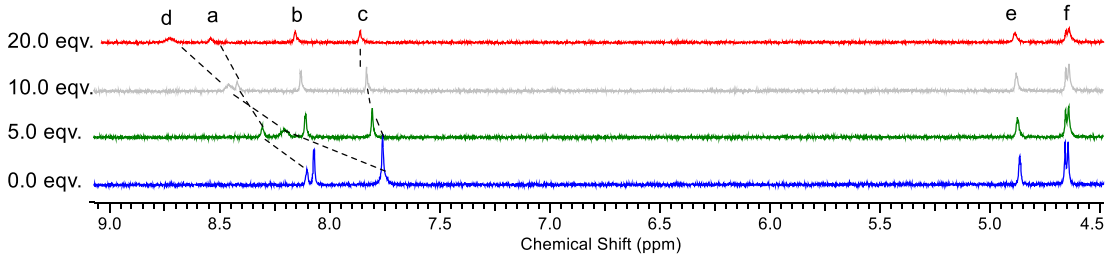

Figure S8. Partial ^{1}H NMR spectra of receptor **1.HB** in CD_3CN/D_2O (99:1 *v*/*v*) in the presence of 0.0, 1.0, 5.0 and 10.0 equivalents of TBACl (400 MHz, 298 K).

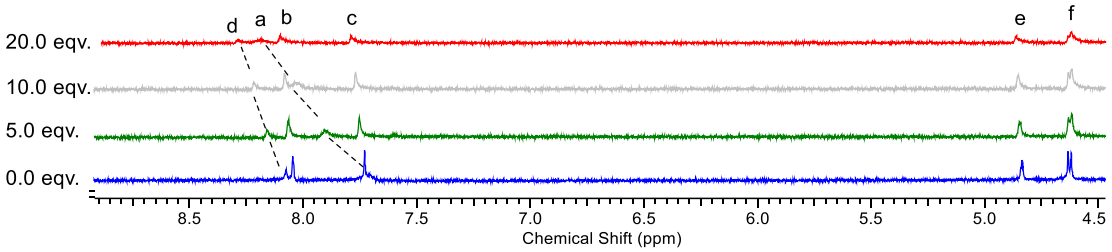

Figure S9. Partial ^{1}H NMR spectra of receptor **1.HB** in CD_3CN/D_2O (99:1 *v*/*v*) in the presence of 0.0, 1.0, 5.0 and 10.0 equivalents of TBABr (400 MHz, 298 K).

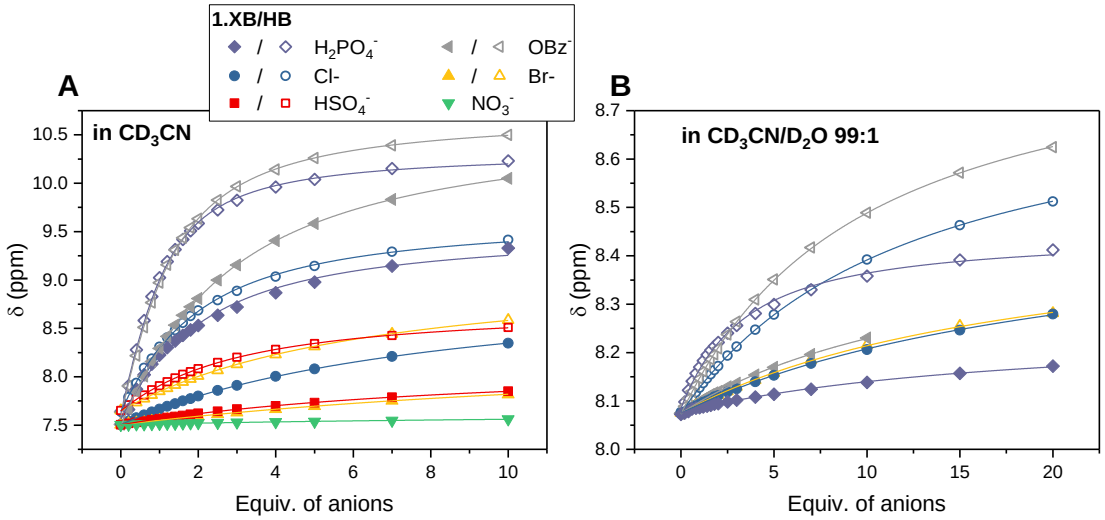

Figure S10. Chemical shifts of A) The amide proton H_d of receptor **1.XB/HB** in CD_3CN and B) The internal isophthalamide proton H_a of receptor **1.XB/HB** in CD_3CN/D_2O (99:1 *v*/*v*) as function of the concentrations of various anions. Filled symbols represent **1.XB**, empty symbols represent **1.HB**. Solid lines represent fits according to a 1:1 stoichiometric host-guest model.

S4 Diffusive Electrochemical Studies

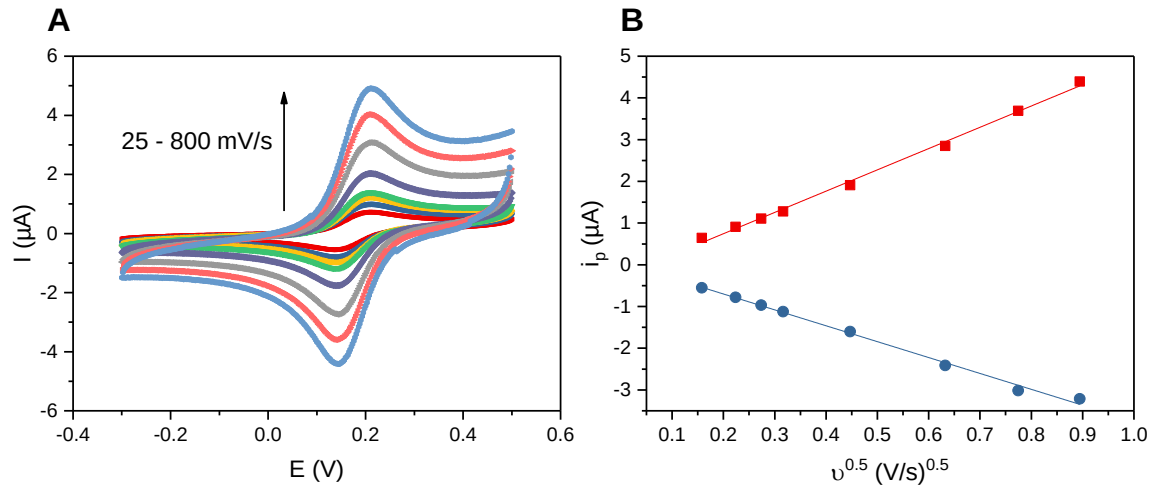

Figure S11. A) CVs at varying scan rate of 0.1 mM **1.HB** in ACN, 100 mM $TBAClO_4$. B) The associated anodic and cathodic peak currents as a function of the square-root of the scan rate including linear fits.

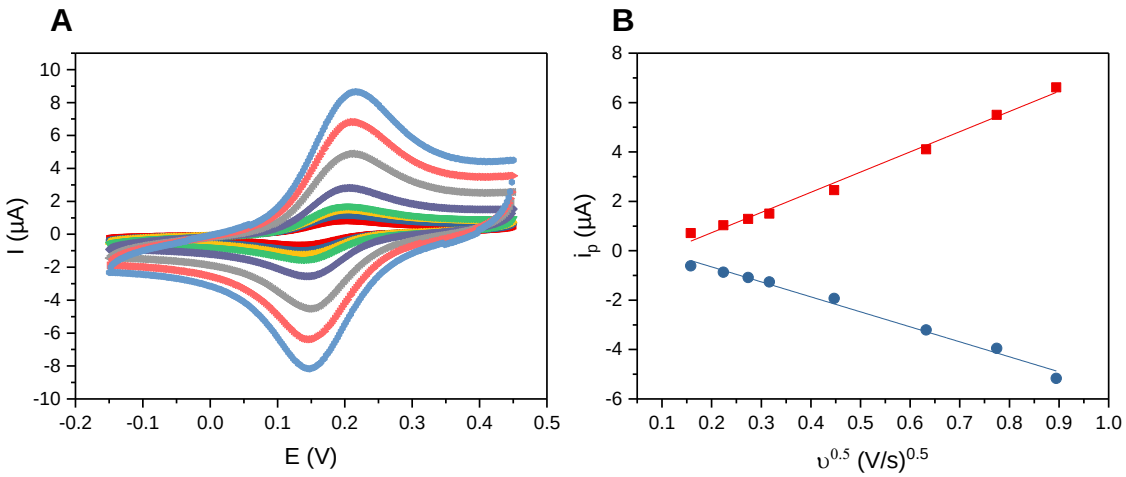

Figure S12. A) CVs at varying scan rate of 0.1 mM **1.XB** in ACN, 100 mM $TBAClO_4$. B) The associated anodic and cathodic peak currents as a function of the square-root of the scan rate including linear fits.

$$\Delta E = -\frac{RT}{nF}\ln\left(\frac{K_{Ox}}{K_{Red}}\right) \qquad \text{eqn. 1}$$

$$\Delta E = -\frac{RT}{nF}\ln\left(\frac{1+K_{Ox}[A^-]}{1+K_{Red}[A^-]}\right) \qquad \text{eqn. 2}$$

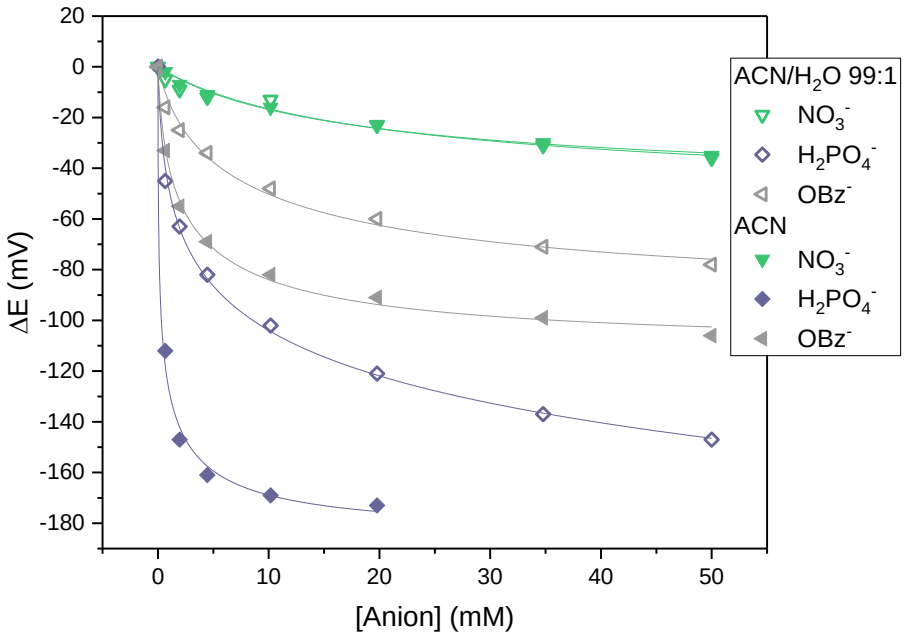

Figure S13. Cathodic voltammetric shifts of **1.XB** in ACN (filled symbols) or ACN/H_2O 99:1 (empty symbols) upon titration with NO_3^-, $H_2PO_4^-$ or OBz^-. Solid lines represent fits to a 1:1 host-guest Nernst model (eqn. 2).

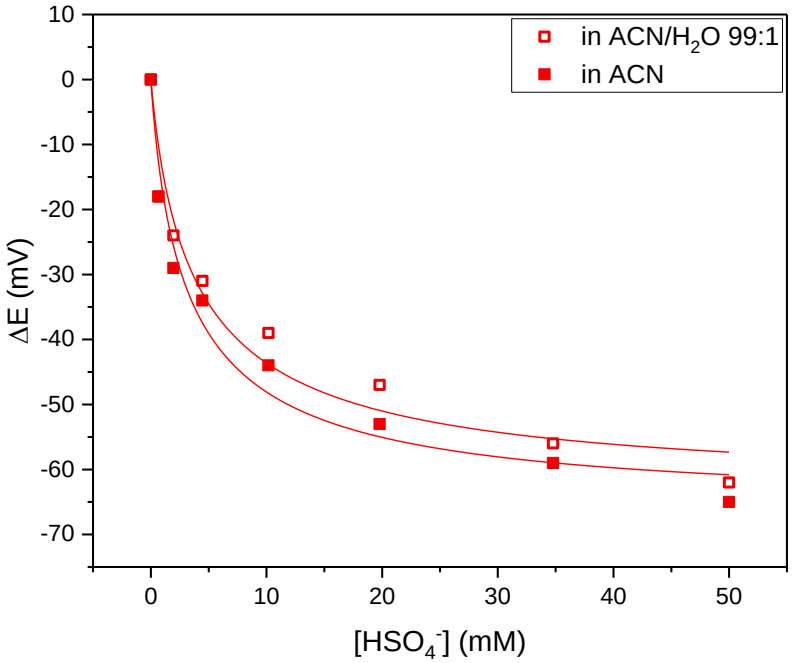

Figure S14. Cathodic voltammetric shifts of **1.XB** in ACN (filled symbols) or ACN/H_2O 99:1 (empty symbols) upon titration with HSO_4^-. Solid lines represent fits to a 1:1 host-guest Nernst model (eqn. 2).

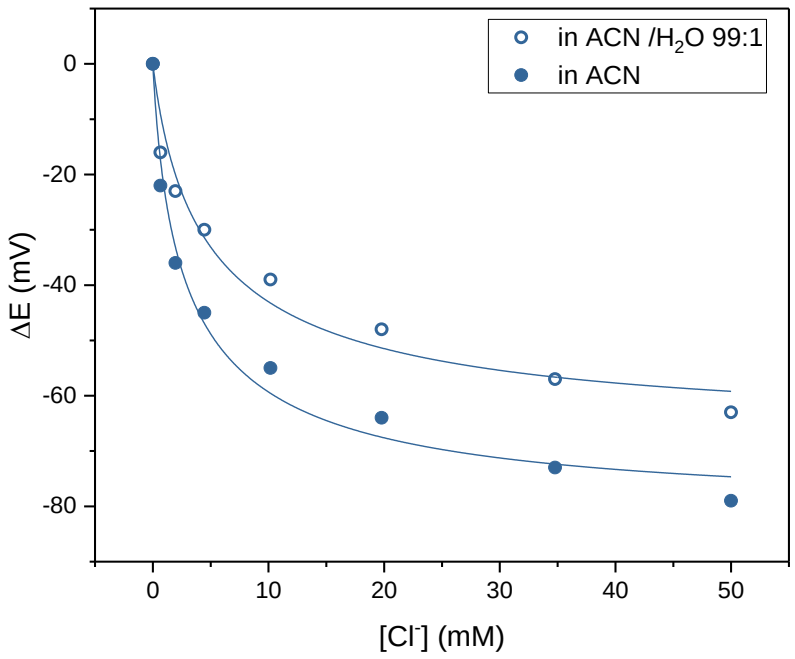

Figure S15. Cathodic voltammetric shifts of **1.XB** in ACN (filled symbols) or ACN/H_2O 99:1 (empty symbols) upon titration with Cl^-. Solid lines represent fits to a 1:1 host-guest Nernst model (eqn. 2).

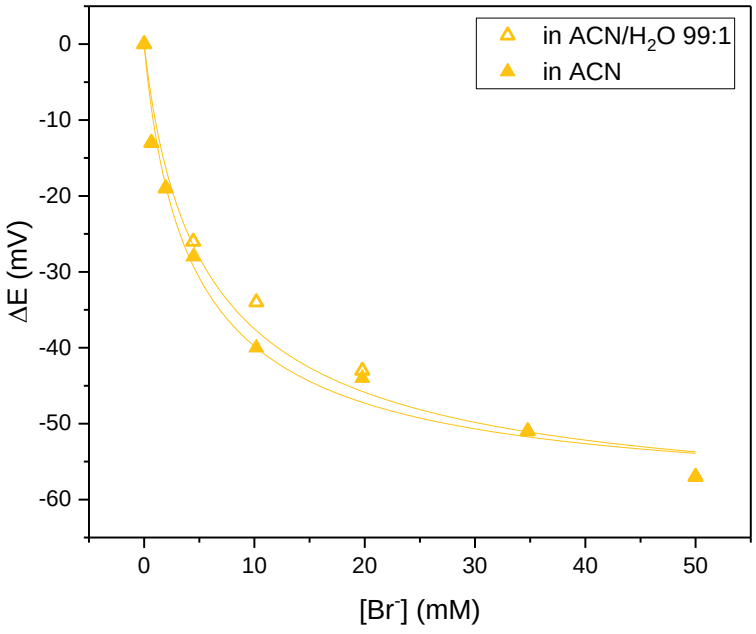

Figure S16. Cathodic voltammetric shifts of **1.XB** in ACN (filled symbols) or ACN/H_2O 99:1 (empty symbols) upon titration with Br^-. Solid lines represent fits to a 1:1 host-guest Nernst model (eqn. 2).

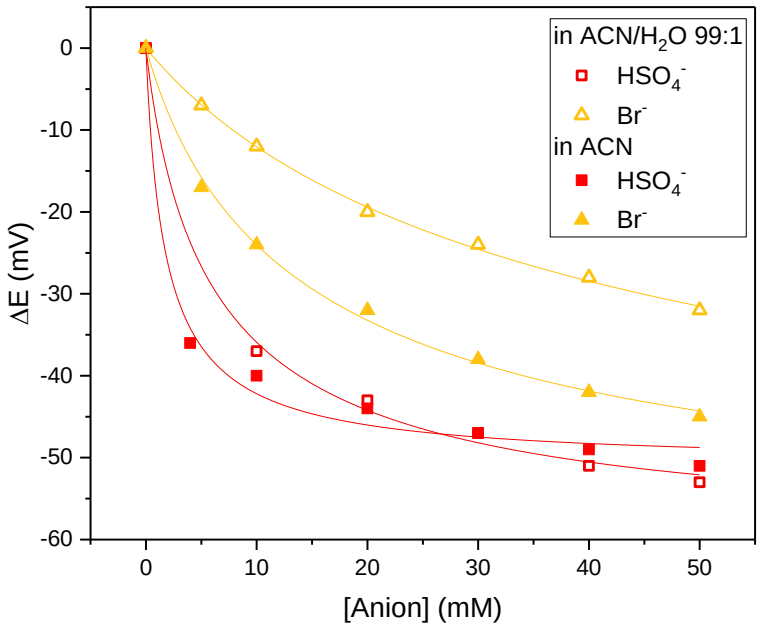

Figure S17. Cathodic voltammetric shifts of **1.HB** in ACN (filled symbols) or ACN/H_2O 99:1 (empty symbols) upon titration with HSO_4^- or Br^-. Solid lines represent fits to a 1:1 host-guest Nernst model (eqn. 2).

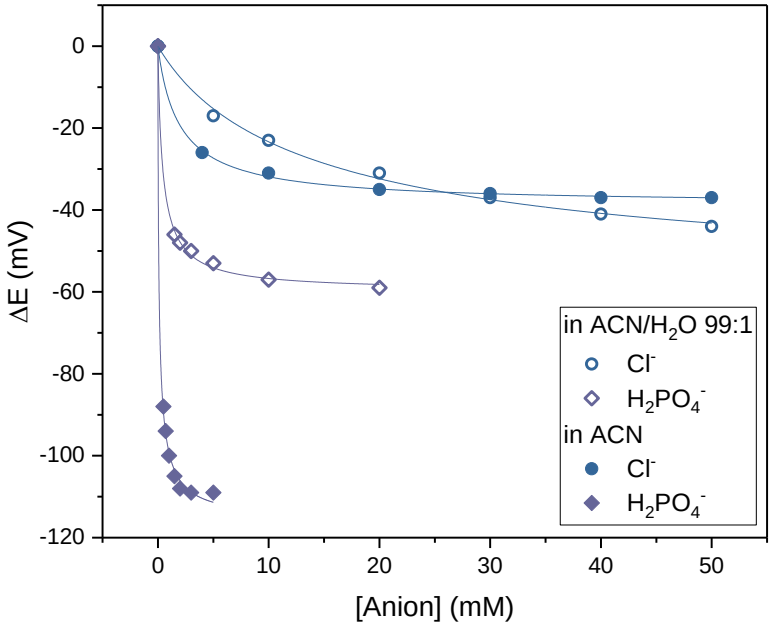

Figure S18. Cathodic voltammetric shifts of **1.HB** in ACN (filled symbols) or ACN/H_2O 99:1 (empty symbols) upon titration with $H_2PO_4^-$ or Cl^-. Solid lines represent fits to a 1:1 host-guest Nernst model (eqn. 2).

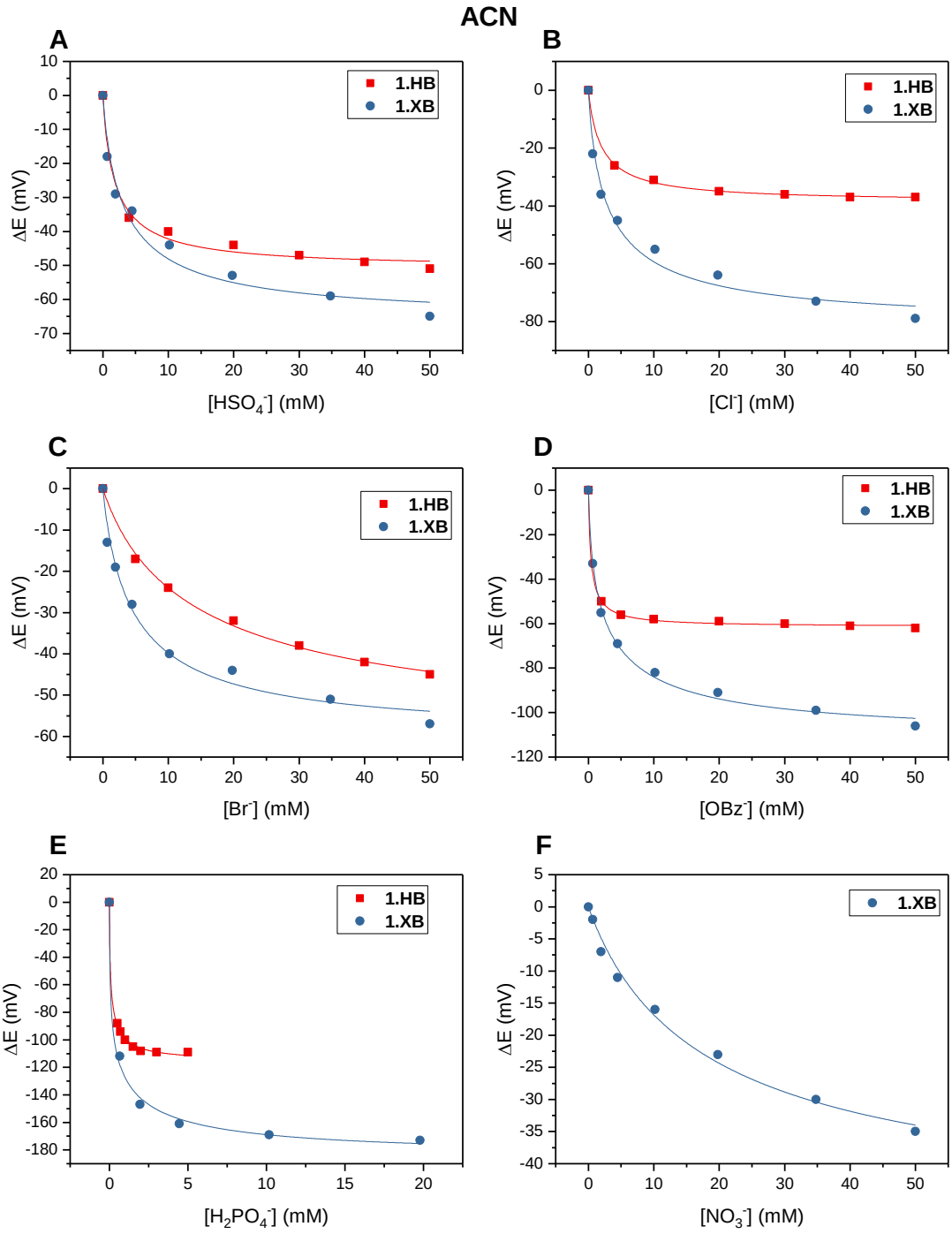

Figure S19. Cathodic voltammetric shifts of **1.XB** (blue circles) and **1.HB** (red squares) in ACN upon titration with various anions: A) HSO_4^-, B) Cl^-, C) Br^-, D) OBz^-, E) $H_2PO_4^-$ and F) NO_3^-. For isotherms that are not shown the binding/response was negligible. [1.XB/HB] = 0.1 mM with 100 mM $TBAClO_4$ supporting electrolyte. The overall ionic strength was kept constant at 100 mM throughout. Solid lines represent fits to a 1:1 host-guest Nernst model (eqn. 2). Note the different y-axis scaling for the graphs.

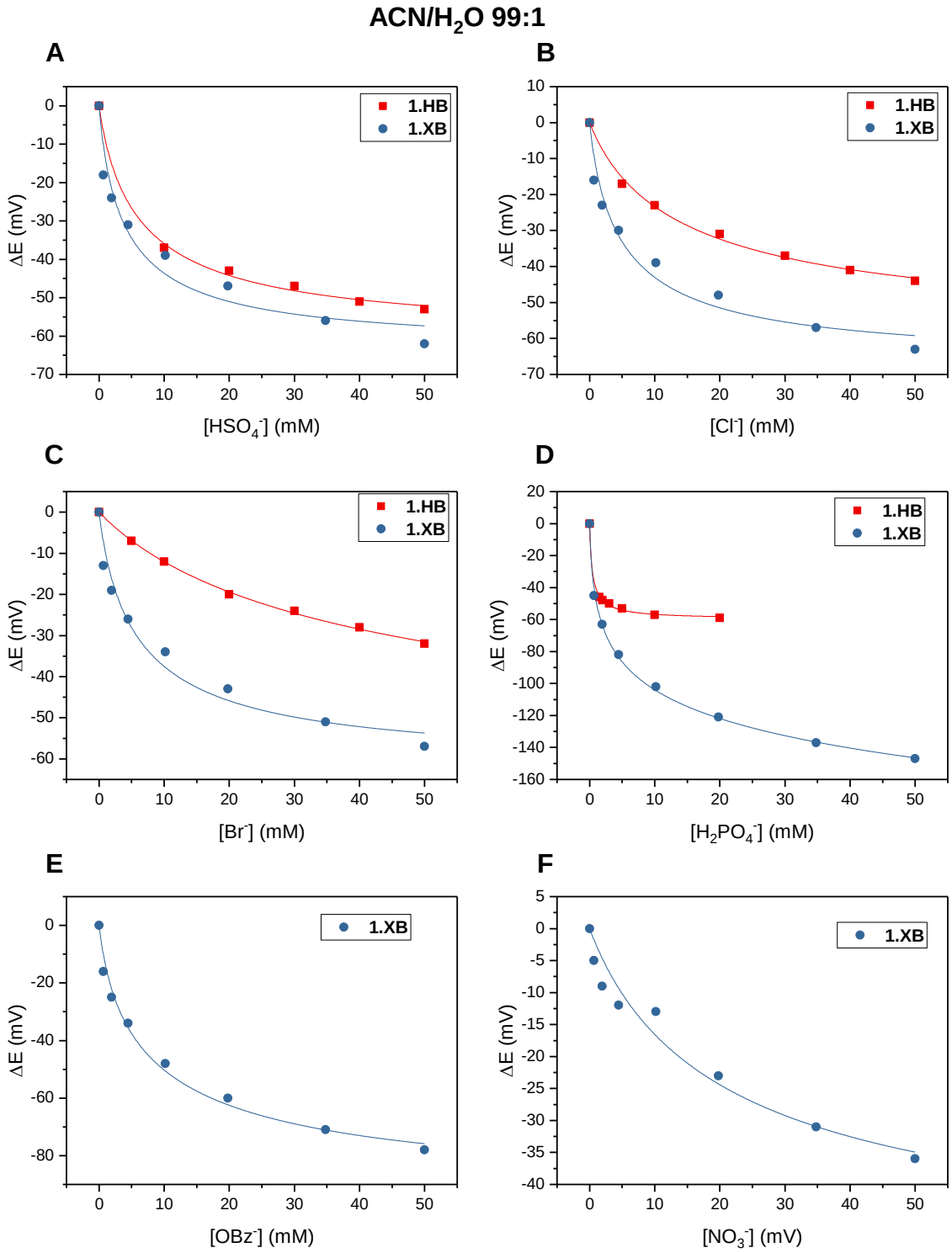

Figure S20. Cathodic voltammetric shifts of **1.XB** (blue circles) and **1.HB** (red squares) in ACN/H_2O 99:1 upon titration with various anions: A) HSO_4^-, B) Cl^-, C) Br^-, D) $H_2PO_4^-$, E) OBz^- and F) NO_3^-. For isotherms that are not shown the binding/response was negligible. [1.XB/HB] = 0.1 mM with 100 mM $TBAClO_4$ supporting electrolyte. The overall ionic strength was kept constant at 100 mM throughout. Solid lines represent fits to a 1:1 host-guest Nernst model (eqn. 2). Note the different y-axis scaling for the graphs.

Table S1. Qualitative comparison of **1.XB** and **1.HB** for the solution phase recognition and sensing of anions in ACN and ACN/H_2O 99:1. Where **1.HB** outperforms **1.XB** the entries are coloured in red while they are coloured in green for XB > HB. In all cases data analysis was performed according to a 1:1 host-guest fit.

Solvent	Anion	K (NMR)	K_{Red}	K_{Ox}	BEF	ΔE
ACN	Cl^-	HB > XB	HB > XB	XB > HB	XB > HB	XB > HB
	Br^-	HB > XB	XB > HB	XB > HB	XB = HB	XB > HB
	HSO_4^-	HB > XB	HB > XB	HB > XB	XB > HB	XB > HB
	$H_2PO_4^-$	HB > XB	HB > XB	XB > HB	XB > HB	XB > HB
	OBz^-	HB > XB	HB > XB	HB > XB	XB > HB	XB > HB
	NO_3^-	XB > HB	XB > HB	XB > HB	/	XB > HB
ACN/H_2O 99:1	Cl^-	HB > XB	XB > HB	XB > HB	XB > HB	XB > HB
	Br^-	HB > XB	XB > HB	XB > HB	HB > XB	XB > HB
	HSO_4^-	/	XB > HB	XB > HB	XB > HB	XB > HB
	$H_2PO_4^-$	HB > XB	HB > XB	HB > XB	XB > HB	XB > HB
	OBz^-	HB > XB	XB > HB	XB > HB	/	XB > HB
	NO_3^-	/	XB > HB	XB > HB	/	XB > HB

S5 Comparison of NMR and Voltammetric Binding Constants

As mentioned in the main text, the anion binding strength, as resolved by ^{1}H NMR titrations does not directly correlate with the response magnitude. While $H_2PO_4^-$ elicited the largest voltammetric response and also displayed the strongest binding in all cases, this correlation is poor for other anions, in particular in the more competitive solvent system. For example, in the ^{1}H NMR titration experiment CD_3CN/D_2O 99:1, HSO_4^- did not elicit any binding to either **1.XB/HB**, however both receptors displayed a significant voltammetric response towards this anion. In contrast, in the same solvent system OBz^- was bound comparatively strongly by both native receptors, however did not induce any perturbation of the Fc/Fc^+ couple of **1.HB**. In CD_3CN the ^{1}H NMR anion binding strength correlates somewhat better with the magnitude of the cathodic perturbations, however both trends are not fully identical. These deviations can most likely be attributed to 1) a different signal transduction and 2) a slightly different solvent system where in the electrochemical titrations non-deuterated solvents are utilised and excess of supporting electrolyte is present. While the supporting electrolyte is not expected to bind to the receptor (and thus compete with anion binding) it has to be noted that the presence of large concentrations of ions certainly affects the dielectric constant of the medium, in turn potentially affecting anion binding.

As can be seen in Tables S2 and S3, the anion binding constants to the neutral receptors as obtained by either ^{1}H NMR or voltammetric titrations are, in most cases, very similar (typically ≤2 fold difference). However, there are some notable exceptions (e.g. BzO^- for **1.XB** in ACN, Br^- for **1.HB** in ACN/H_2O 99:1), where the deviation is significantly larger (≈8 fold difference). These larger deviations can most likely be attributed to larger uncertainties of K_{Red}, in particular when K_{Red} is close to 0.

Interestingly, in ACN the electrochemically determined binding constants (K_{Red}) are typically somewhat underestimated with respect to K_{NMR}. Conversely, in the more competitive ACN/H_2O 99:1 significant anion binding to the neutral oxidation state is sometimes inferred from K_{Red} where NMR experiments indicate negligible binding (e.g. Br^-, HSO_4^-, NO_3^- for **1.XB** in ACN/H_2O 99:1).

Table S2. Comparison of anion binding constants to the neutral receptors **1.XB/HB** obtained by ^{1}H NMR titrations (K_{NMR}; in CD_3CN) and electrochemical titrations (K_{Red}; in ACN, 100 mM $TBAClO_4$).

	1.XB			**1.HB**		
	K_{NMR}	**K_{Red}**	**Ratio**	**K_{NMR}**	**K_{Red}**	**Ratio**
Cl^-	110	68	1.62	340	222	1.53
Br^-	38	66	0.58	75	20	3.75
HSO_4^-	91	85	1.07	196	201	0.98
$H_2PO_4^-$	638	121	5.27	2110	1090	1.94
NO_3^-	16	20	0.80	n. b.	n. b.	/
BzO^-	422	52	8.12	1380	746	1.85

Table S3. Comparison of anion binding constants to the neutral receptors **1.XB/HB** obtained by ^{1}H NMR titrations (K_{NMR}; in CD_3CN/D_2O 99:1) and electrochemical titrations (K_{Red}; in ACN/H_2O 99:1, 100 mM $TBAClO_4$).

	1.XB			**1.HB**		
	K_{NMR}	**K_{Red}**	**Ratio**	**K_{NMR}**	**K_{Red}**	**Ratio**
Cl^-	26	54	0.48	65	21	3.10
Br^-	n. b.	50	/	33	4	8.25
HSO_4^-	n. b.	73	/	n. b.	57	/
$H_2PO_4^-$	37	-2	/	341	715	0.48
NO_3^-	n. b.	16	/	/	/	/
BzO^-	47	20	2.35	89	n. b.	/

S6 Characterization of SAMs

S6.1 X-ray Photoelectron Spectroscopy (XPS)

From XPS the elemental composition of **2.HB$_{SAM}$** was determined, revealing only the presence of C, N, O, S and Fe in the film (Figure S21).

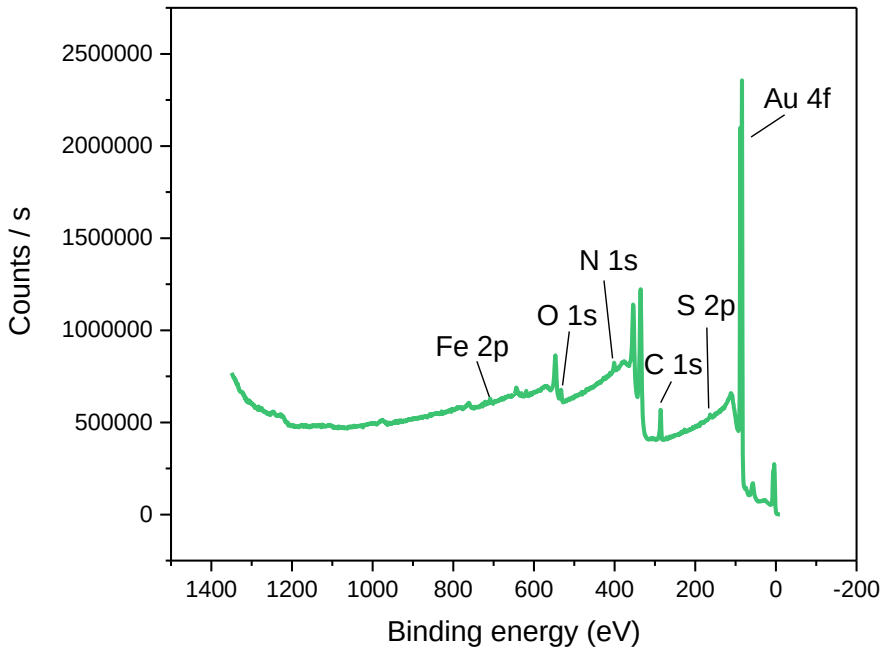

Figure S21. Low resolution survey XPS spectrum of **2.HB$_{SAM}$**. All unassigned peaks arise from other orbitals of the same elements.

Importantly, the atomic ratios obtained from this analysis are in good agreement with the expected values based on the chemical formula of **2.HB** (Table S4).

Table S4. Experimental and theoretical elemental composition of **2.HB$_{SAM}$** determined by XPS. Values were normalised to Fe = 1. Errors represent one standard deviation of triplicate measurements.

	Experimental	Theoretical
C	44.61 ± 1.21	46
N	7.10 ± 0.71	8
O	6.94 ± 0.72	8
S	3.33 ± 0.545	4
Fe	1 ± 0.15	1

From peak fitting of the high resolution C, N and O spectra further information about the specific chemical environments of the receptors can be extracted (Figure S22). In the C 1s high resolution spectrum three distinct chemical environments can be observed and assigned to C−C, C−X (X = N, O, S) as well as C=O bonds.[10-12] The ratio of these peaks roughly reflects the theoretical ratio (Table S5). In the N 1s high resolution spectrum two environments can be observed, one arising from N=N and N−H bond as well as one arising from N−N bonds. These peaks can be assigned based on previous reports of triazole[11] and amide-containing[12] films and their ratio is approximately in line with the expected values.

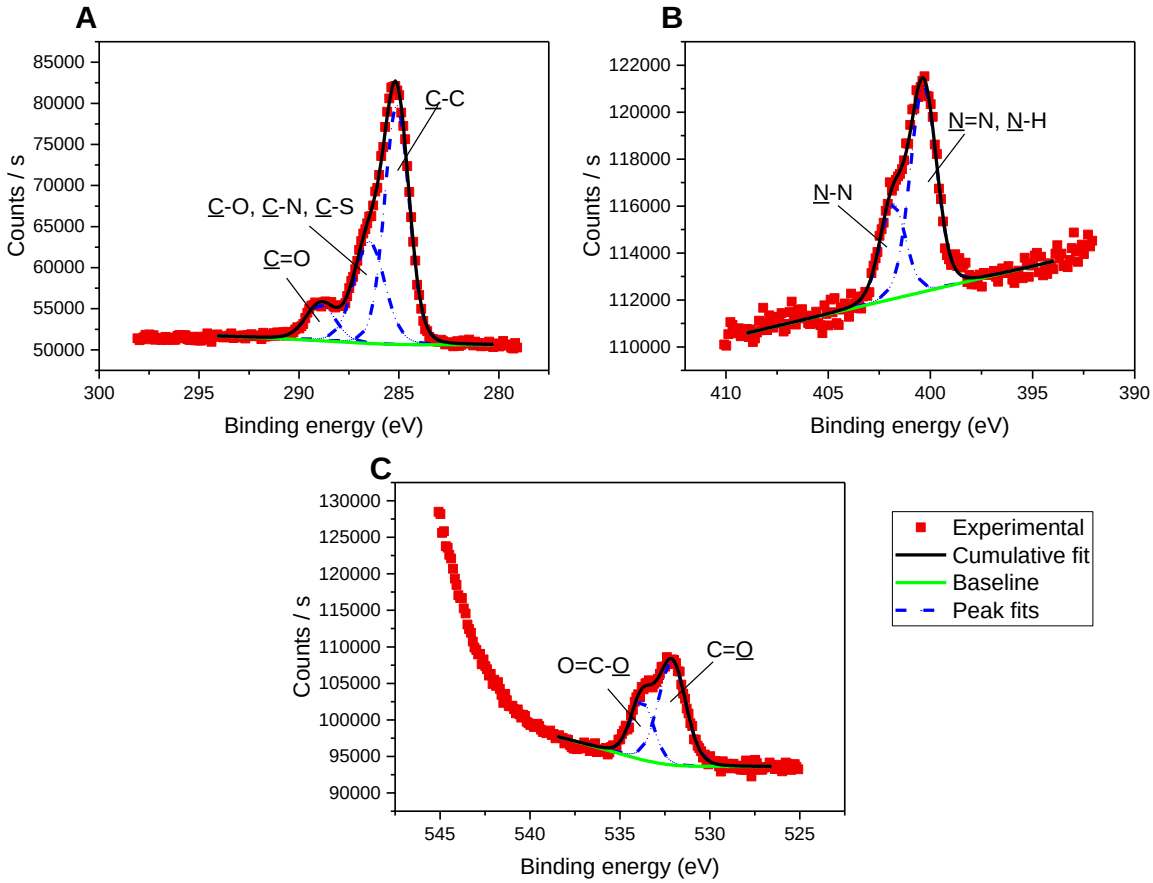

Figure S22. High resolution XPS spectra including peak fits of **2.HB$_{SAM}$**. A) C 1s. B) N 1s C) O 1s.

An excellent agreement with the theoretically predicted peak ratios can be observed for the O 1s peaks assignable to a higher energy O=C–O contribution as well as the carbonyl oxygens.[10]

It should be noted that the different peaks in the S 2p and Fe 2p XPS spectra of **2.HB$_{SAM}$** (Figure S23) are not reflective of different chemical environments around these atoms but arise from spin-orbit coupling. In both cases only one environment is present.

In the high resolution S 2p spectrum two peaks (arising from spin orbit coupling) can be fitted. The binding energies of these peaks of 162.0 eV and 163.5 eV (with a peak separation of 1.5 eV) are in line with previous reports.[13, 14] These results are furthermore indicative of the formation of Au–S interactions (and thus a chemisorbed SAM). For a physisorbed thiol/disulfide a higher binding energy of the S 2p peaks of approx. 165 eV would be observed.[13, 14]

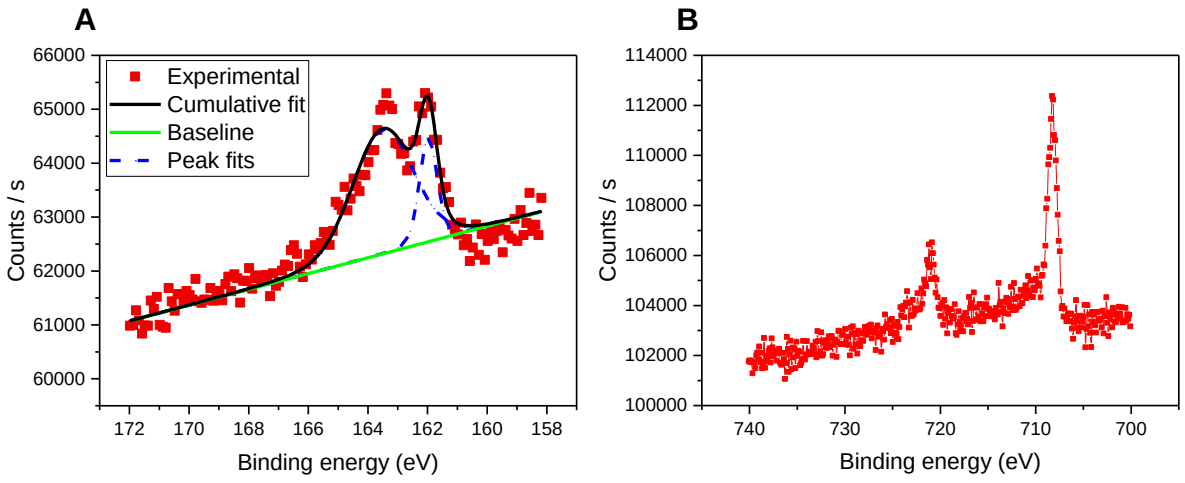

Figure S23. High resolution XPS spectra of **2.HB$_{SAM}$**. A) S 2p. B) Fe 2p. The peaks in both spectra arise from spin orbit coupling and not from chemically different environments.

In summary, XPS confirms the formation of disulfide-tethered SAM, with a chemical composition of functional groups that is consistent with the chemical composition of the receptor.

Table S5. Peak binding energies and experimental and theoretical ratios for different chemical environments of C, N and O of **2.HB$_{SAM}$**. The ratios shown here are obtained by peak fitting of the individual high resolution spectra and do not report on the overall ratio of the elements (see Table SXXX). Errors represent one standard deviation of triplicate measurements.

		Peak BE (eV)	Exp.	Theor.
C	C−C	285.07 ± 0.05	20.57 ± 1.21	28
	C−O, C−N, C−S	286.46 ± 0.05	10.75 ± 1.46	14
	C=O	288.86 ± 0.05	4	4
N	N=N, N−H	400.29 ± 0.11	4.38 ± 1.50	6
	N−N	401.77 ± 0.16	2	2
O	C=O	532.11 ± 0.02	4.17 ± 0.53	4
	(O=C) −O	533.80 ± 0.02	2	2

S6.2 ATR-FTIR spectroscopy

The SAMs were further analysed by attenuated total reflectance Fourier transform infrared spectroscopy (ATR-FTIR). Both **2.XB/HB$_{SAM}$** produced matching spectra, confirming the formation of chemically identical films (Figure S24). A number of functional groups can be observed, including asymmetric and symmetric methylene stretches at 2929 and 2857 cm^{-1}, respectively, in good agreement with previous reports of alkylthiol-based SAMs.[15, 16] Broad peaks at 1740 and 1652 cm^{-1}, most likely arise from ester and amide functional groups, respectively. Another broad signal at 1465 cm^{-1} presumably arises from the triazole moieties.[17] Of note is the prominent peak at 2350 does not arise from the sample but can be assigned to atmospheric CO_2. As there are no significant differences between both SAMs it

can be concluded that bands arising from the C–I bonds in **2.XB$_{SAM}$** fall, as expected for a carbon-halogen single bond, within the fingerprint region.

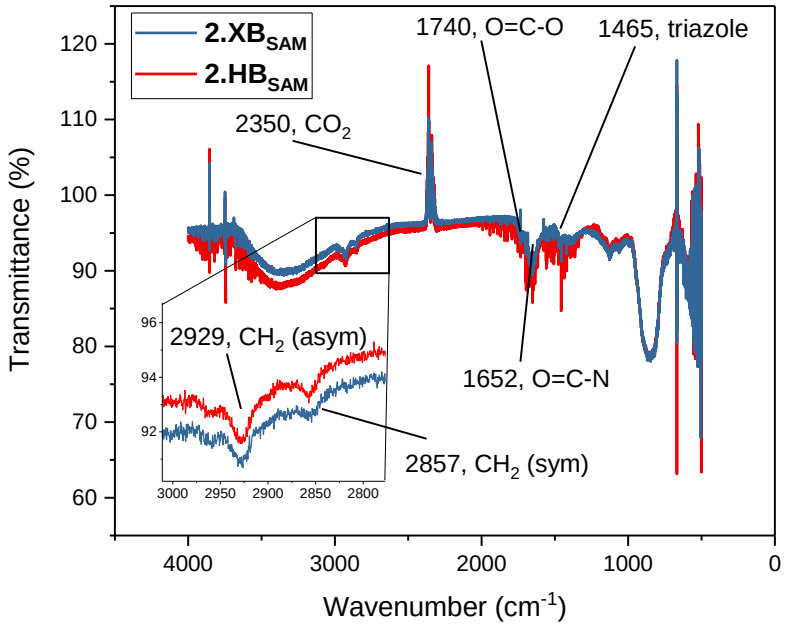

Figure S24. ATR-FTIR spectra of **2.XB/HB$_{SAM}$** on gold.

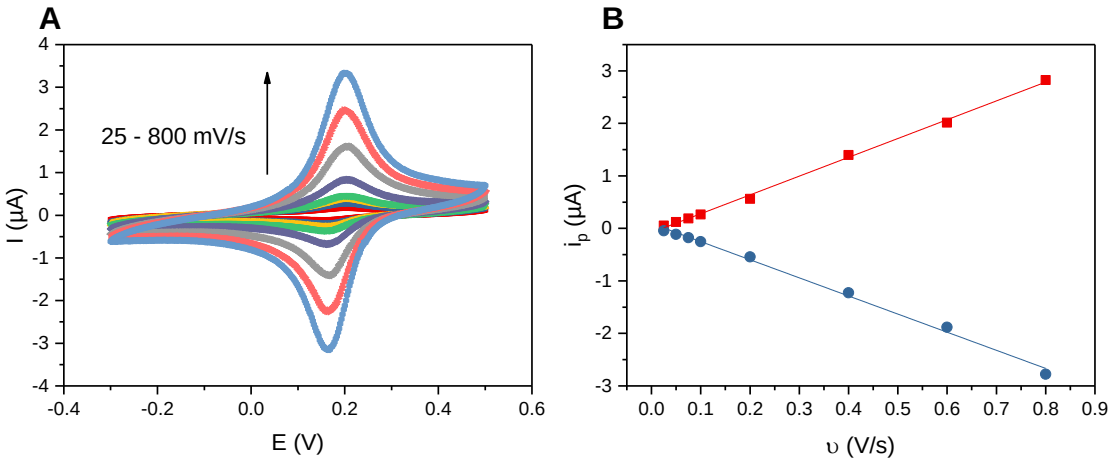

Figure S25. A) CVs at varying scan rate of **2.HB$_{SAM}$** in ACN, 100 mM TBAClO$_4$. B) The associated anodic and cathodic peak currents as a function of the scan rate including linear fits.

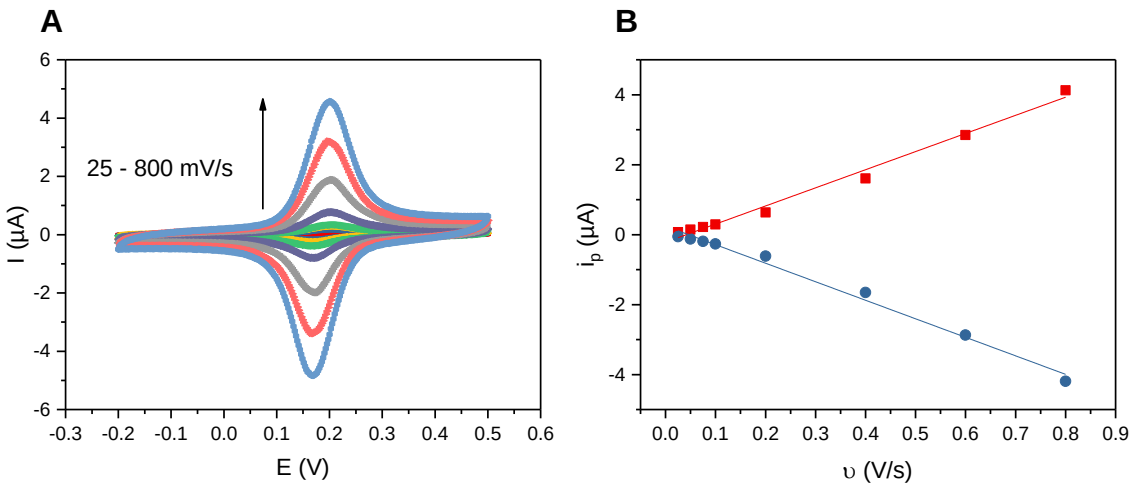

Figure S26. A) CVs at varying scan rate of **2.XB$_{SAM}$** in ACN/H_2O 99:1, 100 mM $TBAClO_4$. B) The associated anodic and cathodic peak currents as a function of the scan rate including linear fits.

Importantly, the electron-density at the Fc is similar in solution as well as in the SAM as the half-wave potentials of both **2.XB$_{SAM}$/1.XB** and **2.HB$_{SAM}$/1.HB** only differ by ≈10 mV, *i.e.* the magnitude of screening of the Fc^+ by the electrolyte is similar in all cases (presumably because the Fc^+ transducer is well exposed to the solution even when-surface confined). This consideration is relevant within the dielectric model as it confirms that the through-bond electron-withdrawing ability of the Fc transducer is near-identical in all environments.

S7 Interfacial Binding Studies

In contrast to solution-phase studies, no systematic anion binding studies were carried with OBz^-, largely as a result of compromised voltammetric stability at higher anion concentrations. Of note is also that the sensing of Br^- is restricted to low concentrations (typically <5 mM) as at higher concentrations the oxidation of Br^- notably overlaps with the Faradaic activity of the Fc-transducer, preventing accurate determination of the peak potentials.

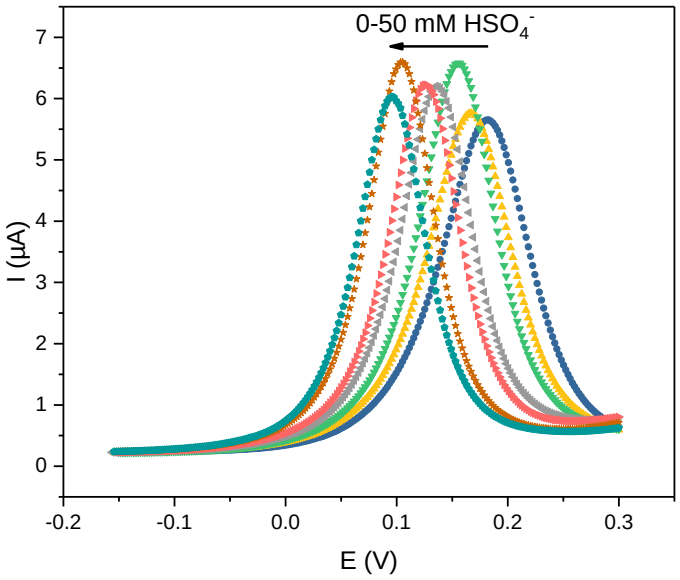

Figure S27. SWVs of **2.XB$_{SAM}$** in ACN/H_2O 99:1 + 100 µM H^+ in the presence of increasing concentrations of HSO_4^-.

Sensing in the presence of acid

As stated in the main text, upon continuous cycling (by CV or SWV) of the SAMs in ACN or ACN/H_2O 99:1 a gradual loss of redox activity is observed. This does, in most cases, not directly impact the sensory behaviour of the films as a the response is only determined by the receptors half-wave potential (herein measured as peak potential in SWV) and not the

peak current magnitude (which is continually and considerably decreasing on subsequent scans while the peak potential typically remains stable). However, over the course of a titration with a significant number of additions, the significant loss of redox activity often results in difficulties in accurately determining peak potentials (e.g. as a result of peak-broadening) and thus may negatively affect the accuracy of the binding isotherms and associated quantifications.

These problems were circumvented by the addition of a small amount of $HClO_4$ (100 μM) which prevents receptor degradation by scavenging nucleophiles (predominantly OH^-, which is known to degrade Fc^+).

This significantly enhances the voltammetric stability of the film (before and during the course of a titration), such that no significant loss of redox activity (and potentially associated peak broadening/uncertainties in peak potentials) is observed (for example, see Figure S27). Importantly, this small acid concentration does not significantly affect anion binding (and thus sensor performance) in almost all cases. For example, the response of **2.HB$_{SAM}$** towards HSO_4^- is largely identical in the absence and presence of acid (Figure S28). For all anions, with the exception of the more basic $H_2PO_4^-$, the binding isotherms are seemingly unaffected by the presence of acid, as shown in the main text, Figure 5. Specifically, the isotherms for HSO_4^-, Cl^-, Br^- and NO_3^- can, in analogy to diffusive studies, be accurately fitted to the standard 1:1 host-guest Nernst model (eqn. 2).

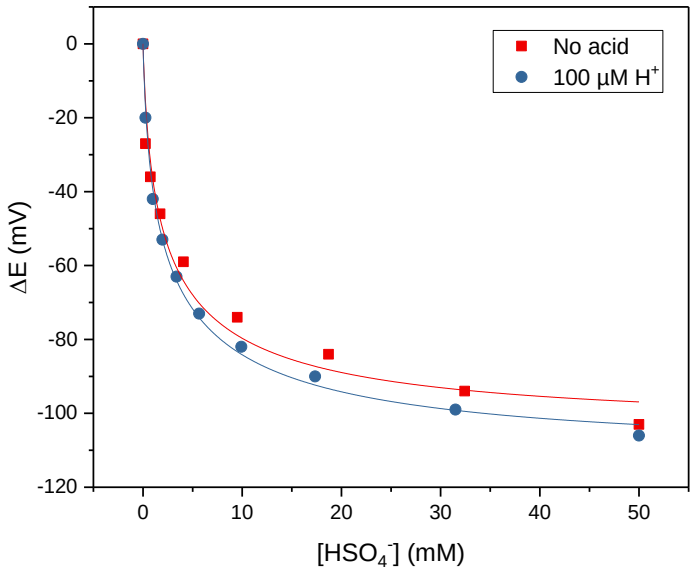

Figure S28. Cathodic voltammetric shifts of **2.HB$_{SAM}$** upon titration with HSO_4^- in ACN/H_2O 99:1, 100 mM $TBAClO_4$, in the absence (red squares) and presence (blue circles) of 100 µM $HClO_4$.

For $H_2PO_4^-$ small deviations are observed for anion concentrations below ≈100 µM (Figure 5B). In this case the anion is protonated to a significant extent when $[A^-] < [H^+]$ (i.e. below ≈100 µM) such that no response is observed (because the neutral H_3PO_4 does not bind to the receptor). At $H_2PO_4^-$ concentrations above 100 µM binding/response is again unaffected and follows the expected Nernst behaviour (eqn. 2). Quantitatively, this shifted (offset) response can be accounted for by fitting the data to eqn. 3 which includes an offset factor Z:

$$\Delta E = -\frac{RT}{nF} * \ln\left(\frac{1+K_{Ox}*([A^-]+Z)}{1+K_{Red}*([A^-]+Z)}\right) \qquad \text{eqn. 3}$$

Eqn. 2.3 was used to obtain binding data for $H_2PO_4^-$ at **2.XB/HB$_{SAM}$** in the presence of 100 µM H^+ (Figure 5B).

S8 Comparison of Diffusive and Interfacial Receptor Response

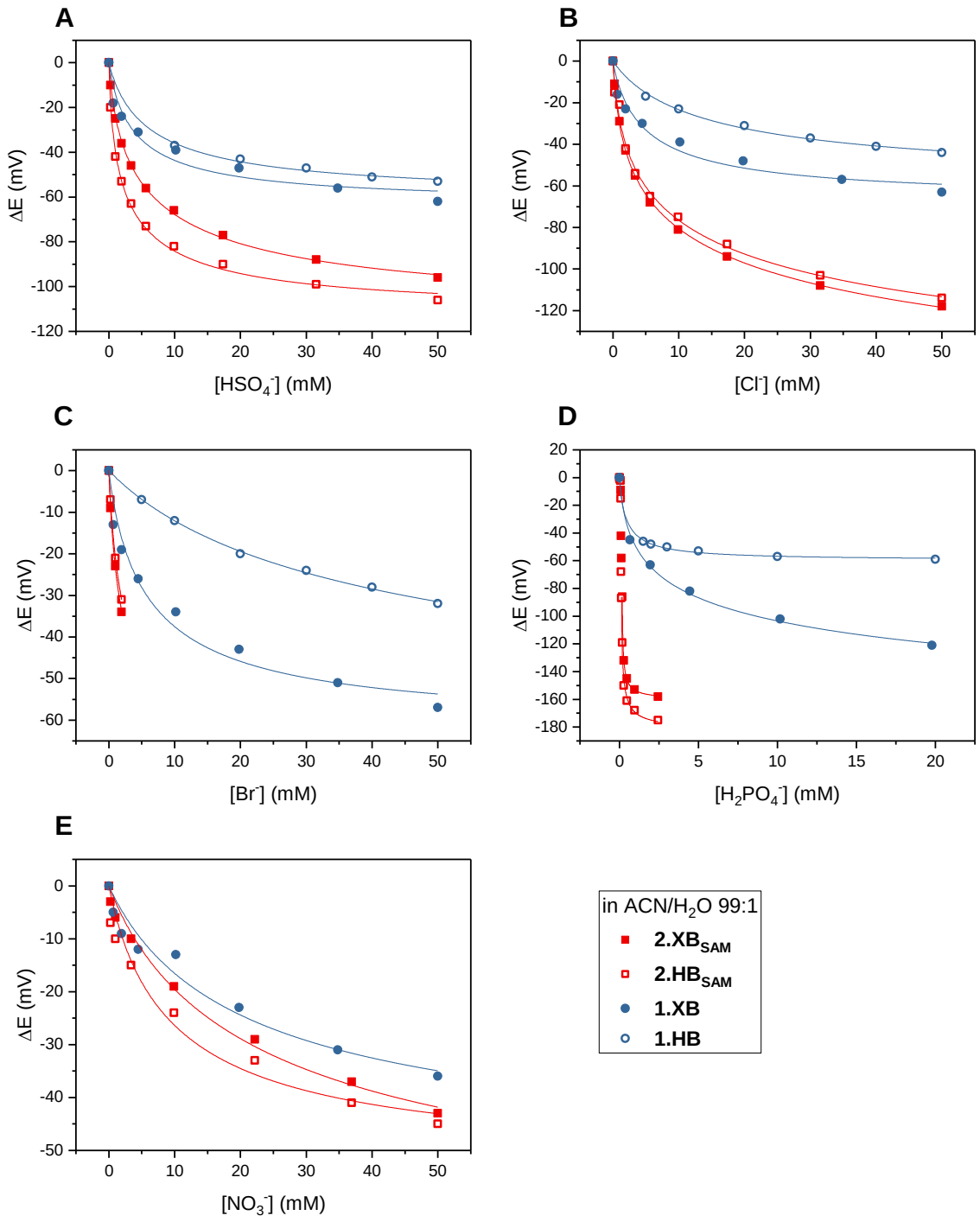

Figure S29. Comparison of cathodic voltammetric shifts under diffusive conditions (**1.XB/HB** (blue circles)) and on the surface (**2.XB/HB$_{SAM}$** (red squares)) in ACN/H_2O 99:1 (+ 100 µM H^+ for SAM titrations) upon titration with various anions: A) HSO_4^-, B) Cl^-, C) Br^-, D) $H_2PO_4^-$ and E) NO_3^-. Filled symbol represent the XB receptors while empty symbols represent the HB receptors. For isotherms that are not shown the binding/response was negligible. Solid lines represent fits to a 1:1 host-guest Nernst model (eqn. 2). Note the different y-axis scaling for the graphs.

In contrast to diffusive studies, the BEFs for both SAMs across various anions is very similar as can be seen in Table 6. No clear differences/trends can be resolved where in most cases the ratio of BEFs for XB/HB SAMs (i.e. the XB enhancement factor) is ≈1, in good agreement with the near-identical response towards anions.

As shown in Table S6 the BEF on the surface is significantly larger in all cases than in solution. For example, BEF enhancement upon immobilisation is greatest for Cl^- with ≈50, the most charge-dense anion. This indirectly supports the proposed screening model, where surface response enhancement is largely driven by coulombic contribution to binding, which will be affected the most by charge-dense anions.
Of further note is that the enhanced interfacial BEF arises from an enhanced interfacial K_{Ox}, while K_{Red} is typically similar, or even smaller than in solution.

Table S6. Ratio of BEF, $\boldsymbol{K_{Ox}}$ and $\boldsymbol{K_{Red}}$ of surface bound (**2.XB/HB$_{SAM}$**) and diffusive receptors (**1.XB/HB**) in ACN/H_2O 99:1 (+ 100 µM H^+ for measurement on SAMs). The absolute binding constants are shown in Table 3 and Table 6.

	Ratio Surface/Solution					
	BEF		**K_{Ox}**		**K_{Red}**	
	XB	**HB**	**XB**	**HB**	**XB**	**HB**
Cl^-	56.7	51.1	3.15	9.74	0.06	0.19
Br^-	1.92	1.49	3.13	19.7	1.64	13.25
HSO_4^-	6.85	8.71	1.88	7.79	0.27	0.90
$H_2PO_4^-$	[a]	[a]	[a]	[a]	[a]	[a]
NO_3^-	1.64	/	1.13	/	0.69	/

a – Errors too large for accurate comparison.

S9 References

1. P. Thordarson, *Chem. Soc. Rev.*, 2011, **40**, 1305-1323.
2. J. Tkac and J. J. Davis, *J. Electroanal. Chem.*, 2008, **621**, 117-120.
3. R. Hein, P. D. Beer and J. J. Davis, *Chem. Rev.*, 2020, **120**, 1888-1935.
4. R. Oliveira, S. Groni, C. Fave, M. Branca, F. Mavre, D. Lorcy, M. Fourmigue and B. Schollhorn, *Phys. Chem. Chem. Phys.*, 2016, **18**, 15867-15873.
5. N. H. Evans, H. Rahman, A. V. Leontiev, N. D. Greenham, G. A. Orlowski, Q. Zeng, R. M. Jacobs, C. J. Serpell, N. L. Kilah and J. J. Davis, *Chem. Sci.*, 2012, **3**, 1080-1089.
6. R. Mishra, S. Pandey, S. Trivedi, S. Pandey and P. S. Pandey, *RSC Adv.*, 2014, **4**, 33478-33488.
7. P. Fortgang, E. Maisonhaute, C. Amatore, B. Delavaux-Nicot, J. Iehl and J. F. Nierengarten, *Angew. Chem. Int. Ed.*, 2011, **50**, 2364-2367.
8. W. S. Brotherton, R. J. Clark and L. Zhu, *J. Org. Chem.*, 2012, **77**, 6443-6455.
9. S. Zhang, Y. Chen, J. Wang, Y. Pan, Z. Xu and C.-H. Tung, *Org. Chem. Front.*, 2015, **2**, 578-585.
10. G. P. López, D. G. Castner and B. D. Ratner, *Surf. Interface Anal.*, 1991, **17**, 267-272.
11. S. Ciampi, T. Böcking, K. A. Kilian, M. James, J. B. Harper and J. J. Gooding, *Langmuir*, 2007, **23**, 9320-9329.
12. G. Zorn, L.-H. Liu, L. Árnadóttir, H. Wang, L. J. Gamble, D. G. Castner and M. Yan, *J. Phys. Chem. C*, 2014, **118**, 376-383.
13. C. D. Bain, H. A. Biebuyck and G. M. Whitesides, *Langmuir*, 1989, **5**, 723-727.
14. D. G. Castner, K. Hinds and D. W. Grainger, *Langmuir*, 1996, **12**, 5083-5086.
15. J. Lehr, J. R. Weeks, A. Santos, G. T. Feliciano, M. I. G. Nicholson, J. J. Davis and P. R. Bueno, *Phys. Chem. Chem. Phys.*, 2017, **19**, 15098-15109.
16. M. D. Porter, T. B. Bright, D. L. Allara and C. E. D. Chidsey, *J. Am. Chem. Soc.*, 1987, **109**, 3559-3568.
17. H. Li, Q. Zheng and C. Han, *Analyst*, 2010, **135**, 1360-1364.